Crystal Structure of *Escherichia coli* ArnA (PmrI) Decarboxylase Domain. A Key Enzyme for Lipid A Modification with 4-Amino-4-deoxy-L-arabinose and Polymyxin Resistance[†,‡]

Petia Z. Gatzeva-Topalova,[§] Andrew P. May,[||] and Marcelo C. Sousa*[,§]

Department of Chemistry and Biochemistry, University of Colorado at Boulder, Boulder, Colorado 80309

Received July 9, 2004; Revised Manuscript Received August 10, 2004

ABSTRACT: Gram-negative bacteria including *Escherichia coli*, *Salmonella typhimurium*, and *Pseudomonas aeruginosa* can modify the structure of lipid A in their outer membrane with 4-amino-4-deoxy-L-arabinose (Ara4N). Such modification results in resistance to cationic antimicrobial peptides of the innate immune system and antibiotics such as polymyxin. ArnA is a key enzyme in the lipid A modification pathway, and its deletion abolishes both the Ara4N-lipid A modification and polymyxin resistance. ArnA is a bifunctional enzyme. It can catalyze (i) the NAD^+-dependent decarboxylation of UDP-glucuronic acid to UDP-4-keto-arabinose and (ii) the *N*-10-formyltetrahydrofolate-dependent formylation of UDP-4-amino-4-deoxy-L-arabinose. We show that the NAD^+-dependent decarboxylating activity is contained in the 360 amino acid C-terminal domain of ArnA. This domain is separable from the N-terminal fragment, and its activity is identical to that of the full-length enzyme. The crystal structure of the ArnA decarboxylase domain from *E. coli* is presented here. The structure confirms that the enzyme belongs to the short-chain dehydrogenase/reductase (SDR) family. On the basis of sequence and structure comparisons of the ArnA decarboxylase domain with other members of the short-chain dehydrogenase/reductase (SDR) family, we propose a binding model for NAD^+ and UDP-glucuronic acid and the involvement of residues T_{432}, Y_{463}, K_{467}, R_{619}, and S_{433} in the mechanism of NAD^+-dependent oxidation of the 4″-OH of the UDP-glucuronic acid and decarboxylation of the UDP-4-keto-glucuronic acid intermediate.

In the process of establishing infections, bacteria must overcome the host defense mechanism including the bactericidal action of cationic antimicrobial peptides (CAMPs).[1] These are small, amphipathic, positively charged peptides that destroy bacteria through membrane permeabilization and constitute a phylogenetically conserved branch of the innate immune system (*1*−*4*). In the case of Gram-negative bacteria, CAMPs bind to the bacterial cell surface through electrostatic interactions with the negatively charged groups of the lipopolysaccharide (LPS), the immunogenic glycolipid in the outer membrane in Gram-negative bacteria (*5*, *6*). They then traverse to the inner membrane and form a pore, which leads to membrane permeabilization and cell death (*7*−*9*). In addition to their function as a key member of the innate immune system, CAMPs represent an important class of clinical antimicrobials. They have both intrinsic bactericidal activity and appear to enhance the activity of other antibiotics, presumably by facilitating their entry into the microbe (*3*, *10*, *11*).

Most Gram-negative bacteria, including *Salmonella typhimurium*, *Escherichia coli*, and the main cystic fibrosis (CF) pathogen *Pseudomonas aeruginosa*, have evolved mechanisms to resist the bactericidal action of CAMPs (*5*, *6*, *12*). These pathogens can modify the structure of lipid A, the anionic, conserved component of LPS in the bacterial outer membrane. The modifications include lipid A acylation and addition of the positively charged sugar 4-amino-arabinose (Ara4N) to lipid A (*5*). Addition of Ara4N to lipid A results in a less negatively charged cell surface, which reduces the electrostatic interactions and, therefore, binding of CAMPs to the bacterial cell surface. It has been clearly shown that the addition of Ara4N to lipid A is responsible for the resistance to polymyxin (an acylated cyclic CAMP) and other CAMPs, such as azurocidin and the bactericidal/permeability-increasing protein (*13*−*15*). Importantly, lipid A from *P. aeruginosa* isolated from CF patients showed modifications with Ara4N (*16*). These modifications confer resistance to the bactericidal action of CAMPs, thus helping the proliferation of the bacteria in the CF lung (*17*).

Modification of lipid A with Ara4N occurs through transcriptional activation of the *pmrE* gene and the seven protein operon *pmrHFIJKLM*. All of these gene products except *pmrM* are essential for the biosynthesis of Ara4N-lipid A and for resistance to CAMPs (*18*). In vitro studies

[†] This work was supported by a grant from the Cystic Fibrosis Foundation and NIH Grant (1 R01 AI060841-01) to M.C.S. Support for P.Z.G.-T. was provided by NIH Training Grant (GM65103).

[‡] Coordinates and structure factors for ArnA decarboxylase have been deposited in the Protein Data Bank as entry 1U9J.

* To whom correspondence should be addressed: Department of Chemistry and Biochemistry, 215 UCB, University of Colorado at Boulder, Boulder, CO 80309. Phone: (303) 735-4341. Fax (303) 492-5894. E-mail: marcelo.sousa@colorado.edu.

[§] University of Colorado at Boulder.

[||] Current address: Fluidigm Corporation. 7100 Shoreline Court, South San Francisco, CA 94080.

[1] Abbreviations: SDR, short-chain dehydrogenase/reductase; CAMPs, cationic antimicrobial peptides; LPS, lipopolysaccharide.

10.1021/bi048551f CCC: $27.50
Published on Web 09/30/2004

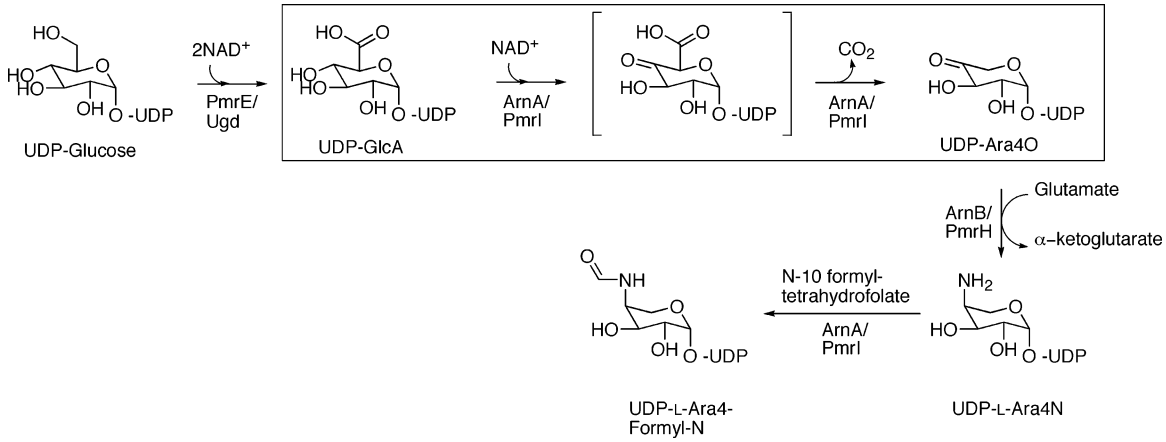

FIGURE 1: Proposed pathway for the biosynthesis of UDP-Ara4N. The pathway starts with Ugd/PmrE oxidizing UDP-Glc to UDP-GlcA. UDP-GlcA is then oxidized at position 4 by the C-terminal domain of ArnA to yield the UDP-4-keto glucuronic acid intermediate that is then decarboxylated to UDP-4-keto arabinose by the same enzyme. UDP-Ara4O is transaminated by ArnB yielding the novel sugar-nucleotide UDP-4-amino-4-deoxy-arabinose (UDP-Ara4N). The N-terminal domain of ArnA can formylate UDP-Ara4N and has been proposed to help displace the reaction catalyzed by ArnB toward UDP-Ara4N synthesis and generate a transiently formylated product (*21*).

by Raetz and co-workers have shown a pathway for the biosynthesis of UDP-L-Ara4N from UDP-glucose (UDP-Glc) (*19*−*21*). The pathway begins with the oxidation of UDP-Glc to UDP-glucuronic acid (UDP-GlcA) catalyzed by the well-characterized UDP-Glc dehydrogenase (PmrE/Ugd) (Figure 1). UDP-GlcA is then oxidatively decarboxylated by ArnA (PmrI) to yield UDP-4-keto-arabinose (UDP-Ara4O), which in turn is transaminated to produce UDP-4-amino-arabinose (UDP-Ara4N) in a reaction catalyzed by ArnB (PmrH). On the basis of sequence similarity to enzymes with known activities, additional gene products of the *pmrHFIJKLM* operon have been proposed to catalyze the transfer of Ara4N from the UDP intermediate to lipid A (*19*, *21*−*24*). The enzymes in this pathway are potential targets for antibacterial drug design. Inhibitors of the pathway would abolish microbial resistance to both CAMPs and cationic peptide antibiotics. Such inhibitors may prove particularly useful in treating chronic infections such as those caused by *P. aeruginosa* in CF patients.

ArnA (formerly, PmrI) is encoded by the *pmrHFIJKLM* operon and is a 74-kDa bifunctional protein. The enzyme can catalyze the transfer of a formyl group from N10-formyl-tetrahydrofolate to UDP-L-Ara4N (*20*, *21*). The N-terminal domain (residues 1−313) is similar in sequence to other enzymes involved in formyl transfer. However, the relevance of this reaction in the biosynthesis of Ara4N-lipid A is unclear. ArnA is also responsible for the C-4″ oxidation of UDP-GlcA to UDP-4-keto-glucuronic acid and its decarboxylation to yield UDP-4-keto-arabinose (boxed in Figure 1) (*20*). The C terminus of ArnA (amino acids 314−660) has sequence similarity to other enzymes that oxidize the C-4″ position of UDP sugars, such as UDP-galactose epimerase, dTDP-glucose-4,6-dehydratase, and UDP-glucuronic acid decarboxylase, all members of the short-chain dehydrogenase/reductase (SDR) superfamily (*25*, *26*). These enzymes use NAD^+ to oxidize the C-4″ hydroxyl of a sugar-nucleotide and recycle the NADH generated to reduce the 4-keto intermediate back to an alcohol (Figure 2). ArnA on the other hand, utilizes NAD^+ as a true substrate, releasing NADH and the UDP-4-keto-sugar as products (*20*) (Figure 2A).

A clear understanding of the ArnA mechanism is crucial for both design and evaluation of selective inhibitors. Here, we show that the C-terminal fragment of ArnA is wholly responsible for the decarboxylation of UDP-GlcA. We thus designate it as the ArnA decarboxylase domain and describe its high-resolution crystal structure. The sequence and structural comparison with other members of the SDR family highlight unique features in ArnA and suggest putative catalytic residues responsible for the decarboxylation step in the conversion of UDP-GlcA to UDP-Ara4O.

MATERIALS AND METHODS

Purification of Full-Length ArnA. The plasmid (pETArnA) for ArnA overexpression was a generous gift from Prof. C. Raetz (*20*). pETArnA was transformed into *E. coli* Nova Blue (DE3) cells (Novagen). A 100 mL overnight culture from a single colony containing 30 μg/mL kanamycin was used to inoculate 6 × 1 L LB medium supplemented with 50 μg/mL kanamycin. Cultures were grown at 37 °C to an OD_{600} of 0.6 and cooled to room temperature before induction with 1 mM IPTG. Cultures were allowed to grow for an additional 3.5 h at room temperature. Cells were harvested by centrifugation at 6000 rpm for 10 min at 4 °C. The cell pellet was resuspended in 100 mL of lysis buffer containing 100 mM HEPES at pH 7.1, 10% glycerol, 500 mM KCl, 5 mM $MgCl_2$, 1 mM PMSF, and 5 mM 2-mercaptoethanol. Lysis was achieved by sonication on ice. Cell debris was removed by centrifugation at 15 000 rpm for 30 min at 4 °C. The supernatant was then applied to a 10 mL Ni-NTA column (Qiagen) previously equilibrated with the above buffer. The column was washed with 5 column volumes of wash buffer containing 50 mM HEPES at pH 7.1, 200 mM KCl, 10% glycerol, 5 mM 2-mercaptoethanol, and 25 mM imidazol at pH 8.0. Elution of the protein from the column was achieved by increasing the concentration of imidazol in the above buffer to 300 mM. Fractions containing the protein were loaded on a size-exclusion (HiLoad 26/60 Superdex 200, Amersham Pharmacia Biotech) column pre-equilibrated with 25 mM Tris-HCl at pH 8.0, 150 mM KCl, 10% glycerol, 1 mM EDTA at pH 8.0, and 5 mM 2-mercaptoethanol and eluted in the same buffer. Elution was monitored by measuring the absorption at 280 nm. The fractions containing

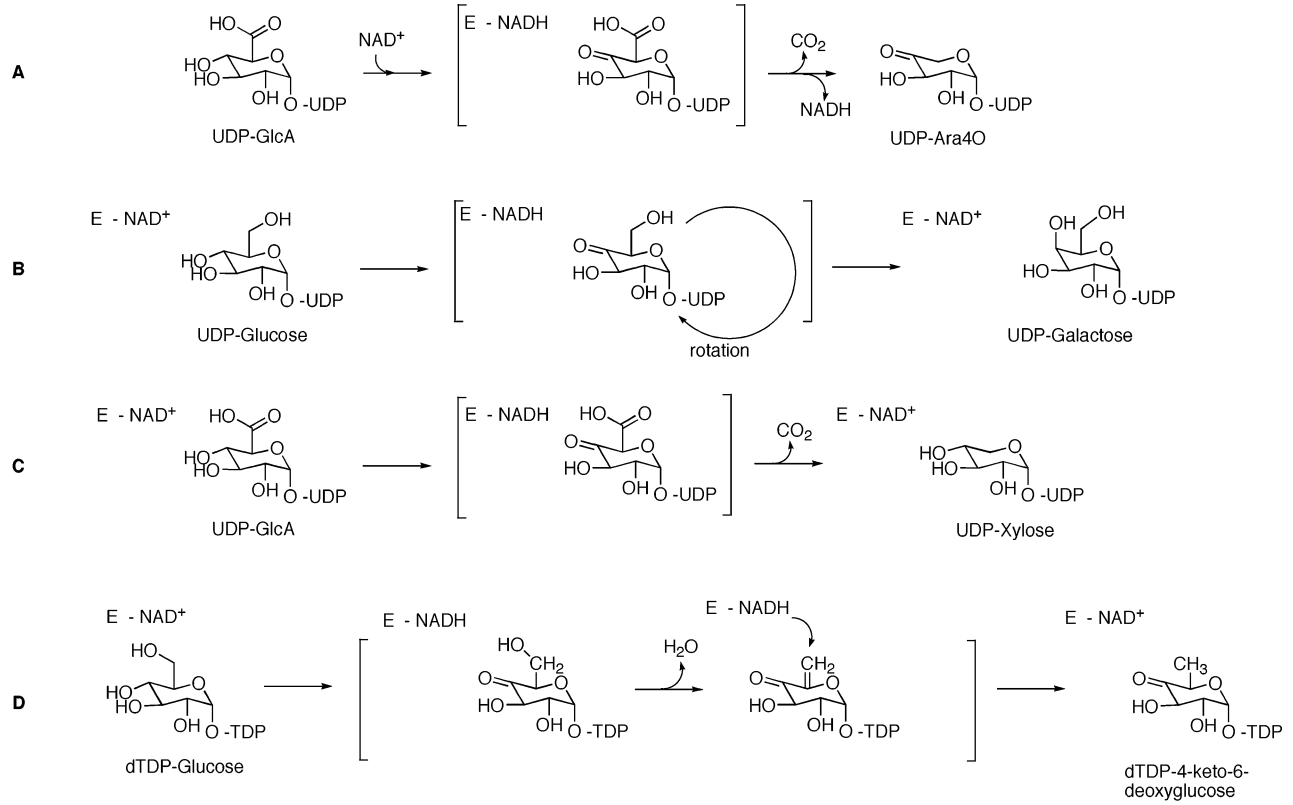

FIGURE 2: Schematic representation of the reactions catalyzed by some SDR enzymes. (A) ArnA decarboxylase domain. (B) UDP-Galactose epimerase. (C) UDP-Glucuronic acid decarboxylase. (D) dTDP glucose-4,6-dehydratase.

protein were combined, and the protein was concentrated to approximately 14 mg/mL (Bio-Rad Protein Assay, Bio-Rad Laboratories). The protein was stored at −80 °C until needed.

Cloning of the ArnA Decarboxylase Domain. The *E. coli* ArnA C terminus was amplified by polymerase chain reaction (PCR) from genomic *E. coli* DNA using the following primers: sense primer, 5′-GTT CAC GCC ATA TGA GCC AGC CTG CCT GCA CCG, containing a *Nde*I restriction site; and antisense primer, 5′-AAG CCT AGA GCT CTC ATG ATG GTT TAT CCG TAA GAT C, containing a *Sac*I restriction site. The PCR amplification was performed with Pfu Turbo polymerase (Invitrogen) according to the instructions of the manufacturer. The PCR product was purified with the QIquick PCR Purification Kit (Qiagen) followed by digestion with *Nde*I and *Sac*I overnight at 37 °C. The digested gene was purified on a 1% agarose gel using the QIquick Gel Purification Kit (Qiagen) and the purified gene ligated into the pMS122 vector [an engineered variant of the pET28 vector that generates an N-terminal His-tag fusion that can be efficiently and specifically cleaved with the Tobacco etch virus (TEV) protease]. The resulting plasmid, pMS159, was sequenced to confirm that no mutations had been introduced in the ArnA C-terminal sequence.

Protein Expression and Purification. The plasmid pMS159 was transformed into *E. coli* Rosetta (DE3) cells (Novagen) and plated on LB media supplemented with 50 μg/mL kanamycin. A total of 100 mL of overnight culture from a single colony containing 50 μg/mL kanamycin was used to inoculate 10 × 1 L LB medium supplemented with 50 μg/mL kanamycin. Cultures were grown at 37 °C to an OD_{600} of 0.6 and cooled on ice to approximately 4 °C. Expression was induced with 0.4 mM isopropyl-β-D-thiogalactopyranoside (IPTG, Gold Bio Technology Inc.), and cultures were allowed to grow overnight at room temperature. Cells were harvested by centrifugation at 6000 rpm for 10 min at 4 °C, and the cell pellet was resuspended in lysis buffer containing 25 mM Tris-HCl at pH 8.0, 5 mM 2-mercaptoethanol, and complete EDTA-free protease inhibitor cocktail used at 1 tablet per 100 mL of buffer (Roche). Cells were lysed on ice by sonication. After lysis, KCl was added to a final concentration of 300 mM and cell debris was removed by centrifugation at 16 000 rpm for 30 min at 4 °C. The supernatant was applied to a 7 mL Ni-NTA column (Qiagen) pre-equilibrated with the lysis buffer containing 300 mM KCl. The column was washed with 5 column volumes of the above buffer, followed by 5 column volumes of wash buffer (25 mM HEPES-KOH at pH 7.5, 300 mM KCl, 10% glycerol, 5 mM 2-mercaptoethanol, and 25 mM imidazole at pH 8.0). The protein was eluted using a 25−300 mM imidazole gradient at pH 8.0 (70 mL final volume). Fractions containing the protein were loaded on a size-exclusion (HiLoad 26/60 Superdex 200, Amersham Pharmacia Biotech) column pre-equilibrated with 25 mM Tris-HCl at pH 8.0, 150 mM KCl, 10% glycerol, 1 mM EDTA at pH 8.0, and 5 mM 2-mercaptoethanol and eluted in the same buffer. Elution was monitored by measuring the absorption at 280 nm. Fractions containing the protein were dialyzed against 25 mM Tris-HCl at pH 8.0 and 5 mM 2-mercaptoethanol and loaded on a MonoQ HR5 column (Pharmacia Biotech) equilibrated in the same buffer. The protein was eluted in buffer containing 25 mM Tris-HCl at pH 8.0, 5 mM 2-mercaptoethanol, and 0−1 M NaCl gradient. The fractions containing protein were combined, and the 6× His tag was removed by overnight incubation at 4 °C with TEV protease (1:50 TEV protease/ArnA) and 10 mM dithiothreitol (DTT). The protein was separated from the protease and the cleaved

Table 1: Data Collection and Refinement Statistics[a]

Data Collection Statistics	
wavelength (Å)	1.54
space group	$P4_132$
cell parameters (Å)	$a = b = c = 150.5$
resolution (Å)	30.0−2.40 (2.49−2.40)
measured reflections	317 340 (27 399)
unique reflections	23 500 (2302)
I/σ	35.0 (5.2)
redundancy	13.5 (11.9)
data completeness (%)	99.3 (100.0)
R_{merge} (%)	7.1 (53.1)
Refinement Statistics	
R_{work}	20.5 (23.5)
R_{free}	24.0 (27.8)
rms deviation from ideal values	
bond lengths (Å)	0.0094
bond angles (deg)	1.4822
dihedrals (deg)	23.1836
improper dihedrals (deg)	0.9882
mean B value (Å^2)	47.4
B factor deviation bonds (Å^2)	1.36
B factor deviation angles (Å^2)	2.19
Ramachandran	
residues in most favored region (%)	90.0
residues in allowed regions (%)	10.0

[a] $R_{work} = \sum|F_{obs} - F_{calc}|/\sum F_{obs}$, where F_{obs} = the observed structure factor amplitude and F_{calc} = the structure factor calculated from the model. R_{free} is computed in the same manner as R_{work}, using the test set of reflections.

tag by size-exclusion chromatography with the column and buffers specified above. The ArnA C terminus was eluted as a monomer from the column. The fractions containing protein were combined, and the protein was concentrated to approximately 10 mg/mL (Bio-Rad Protein Assay, Bio-Rad Laboratories). This protein stock was used for crystallization experiments.

Protein Crystallization and Data Collection. Crystals of the ArnA C terminus were grown by the hanging drop method of vapor diffusion at 16 °C (protein/precipitant, 1.5:1.5 μL). The precipitant was 2.0 M $(NH_4)_2SO_4$, 5 mM DTT, and 100 mM MES at pH 6.75. Crystal growth generally required 4−6 days with crystals having approximate dimensions of 0.3 × 0.3 × 0.3 mm. All of the crystals belonged to the $P4_132$ space group with typical unit-cell dimensions of $a = b = c = 150.5$ Å, $\alpha = \beta = \gamma = 90°$, and 1 molecule per asymmetric unit. Prior to X-ray data collection, the crystals were transferred to cryo-protecting solutions composed of 2.0 M $(NH_4)_2SO_4$, 5 mM DTT, 100 mM MES at pH 6.75, and 5−25% glycerol and flash-cooled in a nitrogen stream. Data were collected with a rotating anode generator using Cu Kα radiation and a Rigaku RAXIS IV^{2+} detector. Data were indexed and integrated with DENZO and scaled with SCALEPACK (*27*). X-ray data collection statistics are shown in Table 1.

Structure Determination and Refinement. The structure of the ArnA C terminus was solved by molecular replacement. The phasing model used was the 2.15 Å refined structure of UDP-galactose 4-epimerase from *E. coli* (PDB ID: 1KVS) (*28*). All non-glycine side chains of the model were set to Ala. Rotation/translation searches, performed with the program AMoRe (*29*) and data between 15 and 5 Å, yielded a solution clearly above the noise level in the space group $P4_132$ but not in the enantiomorphic spacegroup $P4_332$. Inspection of the crystal packing revealed no unfavorable molecular contacts. Using CNS (*30*), 10% of the data was removed for cross validation, and the model was subjected to a round of simulated annealing with torsion-angle dynamics (*31*, *32*). An electron-density map was calculated with data to 2.6 Å resolution. Several side chains were visible in the map and were incorporated into the model using the program O (*33*). The map also revealed sections of the model for which density was not clearly visible, and thus the sections were removed. This new model was again subjected to a round of simulated annealing with torsion-angle dynamics, and model phases were improved by solvent flipping as implemented in CNS (solvent content of 63%). A new map calculated with the improved phases showed unambiguous density for most side chains and connectivity for most of the molecule. The amino acid sequence was readily assigned in this map. The model was subjected to a round of simulated annealing with Cartesian dynamics followed by positional and B-factor refinement with data to 2.4 Å. Manual rebuilding was effected with the program O, and the refinement was continued until no further improvement of the R_{work} and R_{free} was observed (R_{work} of 24.6% and R_{free} of 27.9%). At this point, electron-density maps showed clear density for several solvent molecules and a sulfate ion and were added to the model. Iterative steps of positional and atomic B-factor refinement followed by manual rebuilding were performed until no further improvement of R factors was achieved. The final model (R_{work} of 20.5% and R_{free} of 24.0%) has good stereochemistry as determined using PROCHEK (*34*), with all amino acids laying in the most favorable or allowed regions on the Ramachandran plot. No electron density was observed for residues S605−V616, which are assumed to belong to a conformationally flexible loop. Refinement statistics and model stereochemistry are summarized in Table 1.

Enzyme Assays and Kinetic Studies. The standard reaction mixture contained 25 mM Tris at pH 8.0, 5 mM 2-mercaptoethanol, 0.2 mg/mL BSA, 10% glycerol, 100 mM KCl, 4 mM NAD^+, and 1 mM UDP-glucuronic acid. The reaction was started with the addition of the 200 nM ArnA full-length or C-terminal domain. Enzyme activity was measured by following the absorbance of the produced NADH at 340 nm. All enzyme assays were carried out at 37 °C in a final volume of 800 μL. The initial velocity studies were performed by varying the concentration of NAD^+ from 0.125 to 4.0 mM and keeping UDP-glucuronic acid constant at 1 mM (Figure 3A) or by changing the concentration of UDP-glucuronic acid from 0.031 to 1.0 mM and keeping NAD^+ at 4 mM (Figure 3A).

NAD^+-Dependent Conversion of UDP-GlcA to UDP-Ara4O. Assays were performed as described before with minor modifications (*20*). Briefly, a solution contained 25 mM Tris at pH 8.0 and 5 mM 2-mercaptoethanol with the 0.5 mg/mL purified ArnA full-length or C-terminal domain, 11 μM UDP-GlcA (glucuronyl−^{14}C(U), Perkin−Elmer), and 3 mM NAD^+ (Sigma) at room temperature for 40 min. The above reaction mixture without NAD^+ was used as a control. A total of 0.5 μL of each reaction mixture was then spotted on polyethyleneimine (PEI) cellulose plate prewashed in methanol. The plate was developed in a solvent system containing 0.25 M acetic acid and 0.4 M LiCl. Radioactivity in the plate was visualized with a PhosphorImager.

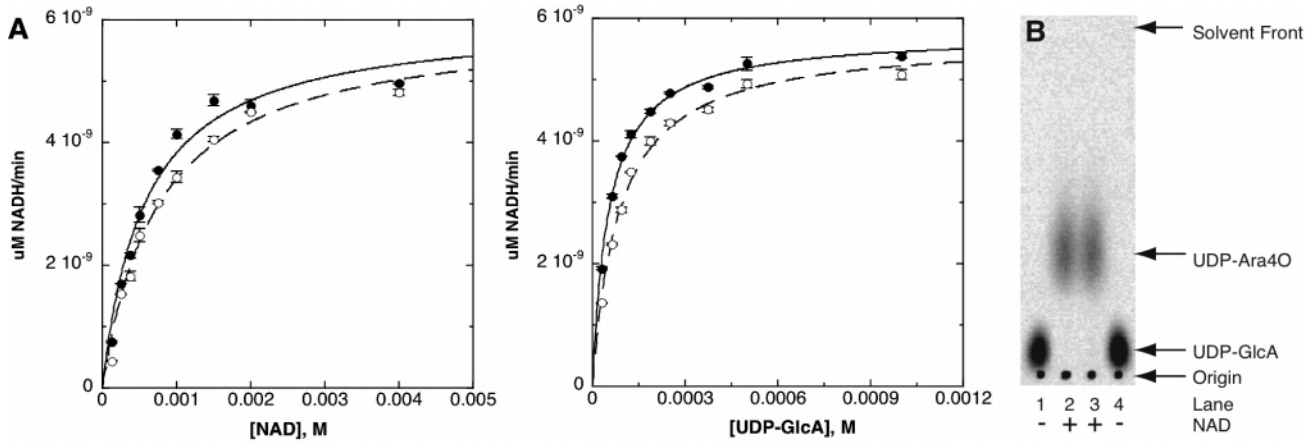

FIGURE 3: Decarboxylase activity of full-length ArnA and its C-terminal domain. (A) Plots of initial velocity versus substrate concentration for full-length ArnA (○) and ArnA C-terminal domain (●). The enzyme activity was measured by monitoring the formation of NADH. (B) Detection of the reaction product UDP-Ara4O by thin-layer chromatography. Lanes 1 and 2, Full-length ArnA; lanes 3 and 4, ArnA C-terminal domain. No formation of UDP-Ara4O is observed in the absence of NAD^+ in the reaction mixture.

RESULTS AND DISCUSSION

The C-Terminal Domain of ArnA Is a UDP-GlcA Decarboxylase. As mentioned previously, ArnA is a bifunctional enzyme with both formyl-transferase and UDP-GlcA decarboxylase activities (*20*). Sequence analysis suggested that the C-terminal fragment of ArnA may represent a separable domain with UDP-GlcA decarboxylase activity. A fragment of *E. coli* ArnA comprising amino acids 306−660 was cloned and overexpressed as a His-tag fusion and purified to homogeneity as described in the Materials and Methods. The His tag was cleaved with TEV protease resulting in an ArnA C-terminal fragment with a three additional amino acids (HGM) at the N terminus.

The UDP-GlcA acid decarboxylation reaction catalyzed by ArnA can be followed spectrophotometrically by measuring the production of NADH (*20*). A comparison of the decarboxylase activity of the ArnA full-length enzyme and its C-terminal fragment shows identical behavior for the two proteins (parts A and B of Figure 3). The apparent K_m values for NAD^+ and UDP-GlcA were 0.76 ± 0.09 and 0.086 ± 0.006 mM for the full-length enzyme and 0.57 ± 0.09 and 0.054 ± 0.003 mM for the C-terminal fragment. The decarboxylated product released by the ArnA full-length enzyme is UDP-4-keto-arabinose (UDP-Ara4O). The conversion of UDP-GlcA into UDP-Ara4O can be detected by thin-layer chromatography, where UDP-Ara4O migrates faster than UDP-GlcA. Using NMR analysis, Breazeale et al. confirmed that the fast-migrating species correspond to UDP-Ara4O (*20*). As shown in Figure 3B, the C-terminal domain of ArnA also produces UDP-Ara4O as detected by thin-layer chromatography. We therefore conclude that the C-terminal fragment of ArnA is responsible for the oxidative decarboxylation of UDP-GlcA. This C-terminal fragment is a separable, functional domain, and from here onward, we shall refer to it as the ArnA decarboxylase domain.

Crystal Structure of the ArnA Decarboxylase Domain. The decarboxylase domain of ArnA described above was crystallized, and the structure was determined to 2.4 Å resolution as described in the Materials and Methods. Data collection and refinement statistics are shown in Table 1.

The overall structure of ArnA decarboxylase domain is distinctly bilobal. It contains a larger N-terminal subdomain

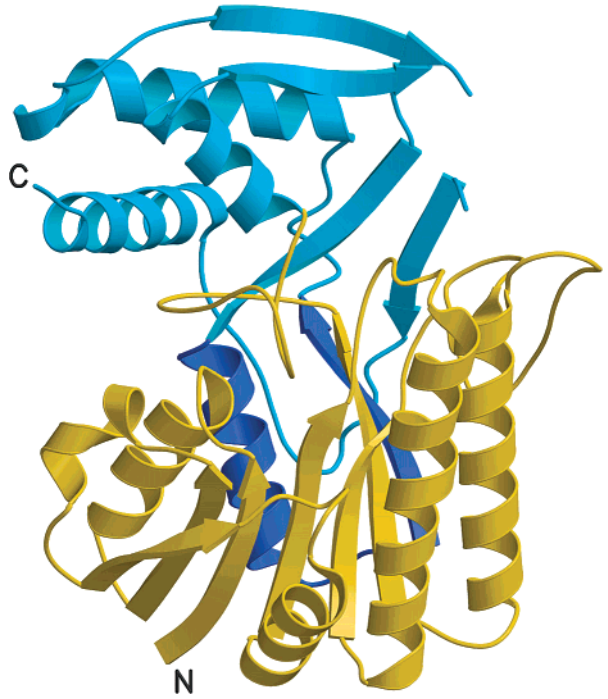

FIGURE 4: Overall structure of the ArnA decarboxylase domain. The N-terminal subdomain (in gold) is formed by residues R_{315}−R_{510} and R_{541}−G_{566}. It adopts a modified version of the classic Rossmann fold in that an α helix and a β strand are donated by the C-terminal subdomain (shown in dark blue). The C-terminal subdomain (in blue) is formed by residues A_{511}−I_{540} and N_{567}−T_{656}. All molecular diagrams were prepared with Molscript (*52*) and rendered with Raster 3D (*53*).

formed by amino acids R_{315}−R_{510} and R_{541}−G_{566} folding into a 7-stranded parallel β sheet sandwiched by three α helices on either side (Figure 4). This represents a modified version of the classic Rossmann fold observed in many dinucleotide-binding proteins in that an α helix and a β strand are donated to the Rossmann fold by the C-terminal subdomain (Figure 4). The smaller C-terminal subdomain is formed by residues A_{511}−I_{540} and N_{567}−T_{656} and consists of four strands of pleated β sheet and three α helices.

The structure of ArnA decarboxylase shown here represents the unliganded form of the enzyme and clearly shows that ArnA decarboxylase belongs to the SDR superfamily (*25*, *26*). This group of proteins is characterized by high

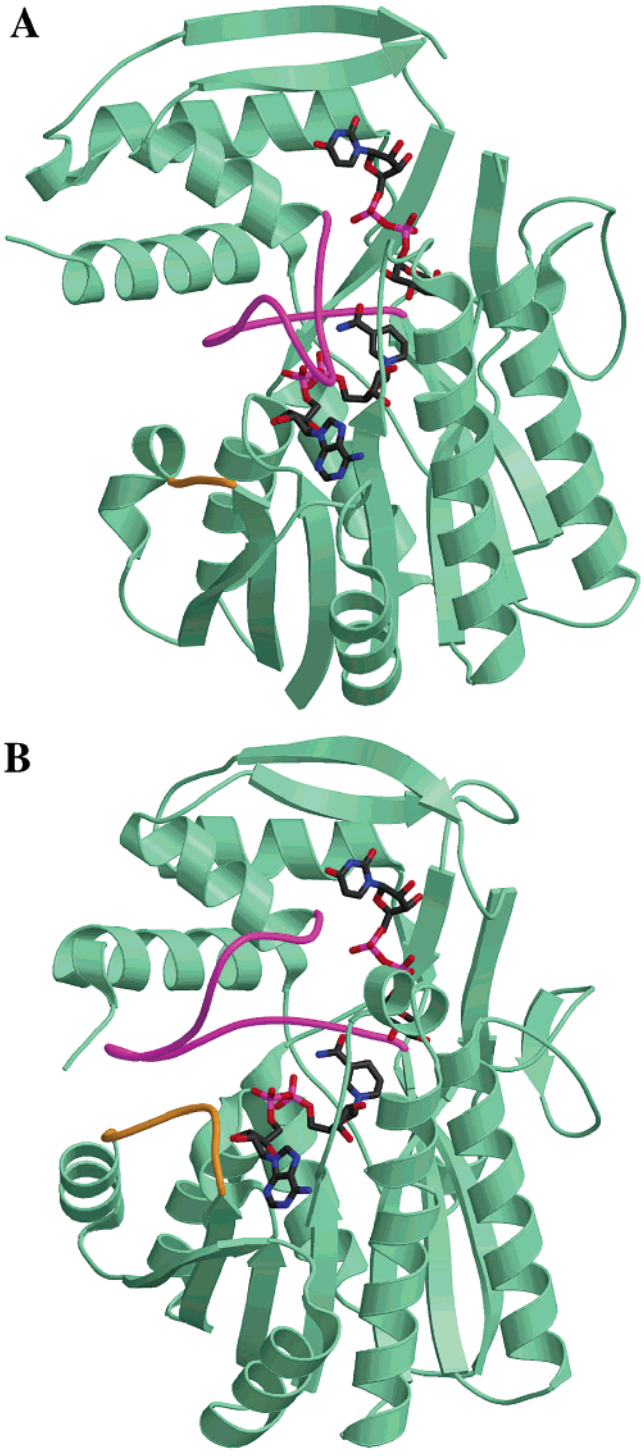

FIGURE 5: (A) Crystal structure of the *E. coli* ArnA decarboxylase domain with substrates modeled in the active site. (B) Crystal structure of *E. coli* UDP-galactose 4-epimerase with its substrates bound in the active site (PDB ID: 1A9Y). The two loops highlighted in magenta and gold in both proteins reveal structural differences likely to be important in substrate binding.

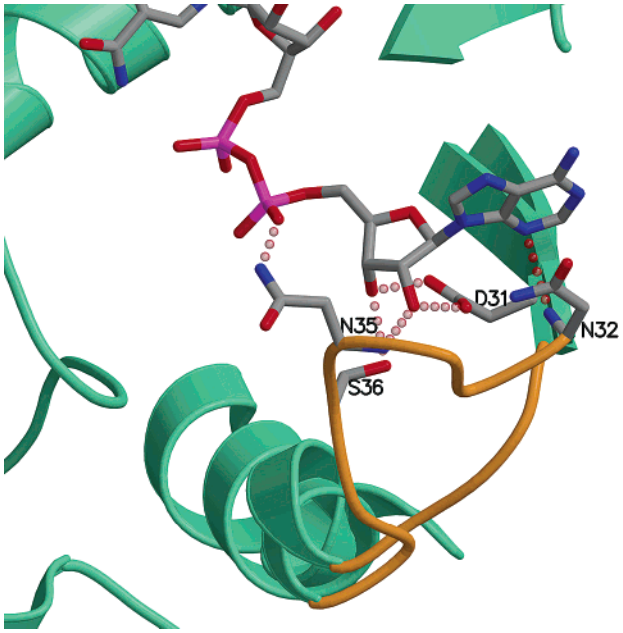

FIGURE 6: Conformational differences between the ArnA decarboxylase domain and UDP-galactose epimerase in the NAD^+-binding loop that contacts the adenine. The loop is highlighted in gold and shows relevant residues in ecGALE hydrogen bonding with the adenine base. There is a four amino acid residue deletion in this loop in ArnA, and its conformation would prevent contact with NAD^+.

structural similarity and the presence of specific sequence motifs despite low overall sequence identity (15−30%). ArnA decarboxylase retains the classical glycine-rich NAD^+-binding motif GX(X)GXXG represented by amino acids $G_{322}VNG_{325}FIG_{328}$. The structure also reveals the presence of a conserved water molecule (HOH 32 in the coordinate file) that normally bridges the dinucleotide with the glycine-rich region and is proposed to be important for dinucleotide binding (*35*). Also important for NAD^+ binding is the presence of a conserved acidic amino acid (D/E) (D_{347} in ArnA) that interacts with adenine ribose hydroxyls and is present in all NAD^+- and FAD-binding members of the SDR family. The characteristic signature sequence YXXXK, which together with a conserved T/S residue forms a catalytic triad that catalyzes the NAD^+-dependent oxidation of a sugar hydroxyl is also present in ArnA, represented by residues T_{432} and $Y_{463}SVSK_{467}$.

Comparison to UDP-Gal Epimerase and Substrate-Binding Model. The *E. coli* UDP-galactose 4-epimerase (ecGALE) has been extensively studied both structurally and kinetically and represents one of the best characterized members of the SDR family (*28*, *36*−*42*). The structures of ArnA and ecGALE share the same overall fold and topology. Despite relatively low overall sequence identity (27%), the structures of the two enzymes superimpose with a root-mean-square (rms) deviation of 1.53 Å for 216 α-carbon atoms in structurally conserved regions (see the Supporting Information for a movie with a superposition of both enzymes). The residues determined to be crucial for NAD^+ binding, as well as those responsible for the 4″-OH oxidation in ecGALE, are conserved in ArnA, both in terms of sequence and structure (in ArnA, $G_{322}G_{325}G_{328}$ and D_{347} for NAD^+ binding; T_{432}, Y_{463}, and K_{467} for UDP-GlcA 4″-OH oxidation). ArnA and ecGALE catalyze identical first steps in their reactions, namely, the NAD^+-mediated oxidation of the hydroxyl group at position C4″ in the UDP-sugar (Figure 2). On the basis of these similarities, we have modeled the substrates NAD^+ and UDP-GlcA in the active site of ArnA decarboxylase, using the positions of NAD^+ and UDP-Glc in ecGALE [PDB ID: 1A9Y, (*42*)] as a guide (Figure 5).

The comparison between the structure of ecGALE in complex with its substrates NAD^+·UDP-Glc and ArnA decarboxylase with NAD^+ and UDP-GlcA modeled in the

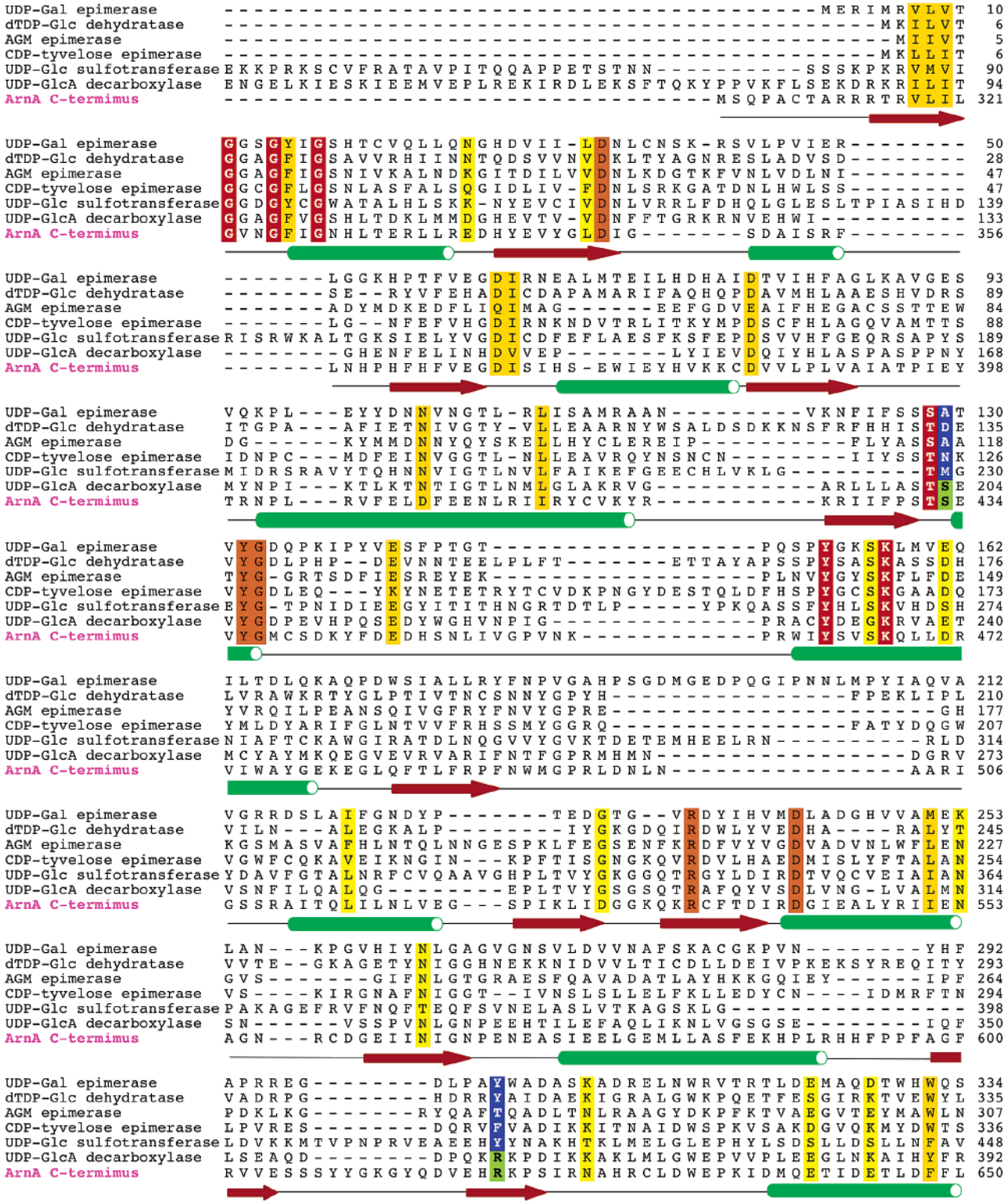

FIGURE 7: Sequence alignment of members of the SDR family and secondary-structure assignment of ArnA decarboxylase. α helices are shown as green cylinders and *β* strands, as red arrows. The proteins are *E. coli* UDP-galactose 4-epimerase (UDP-Gal epimerase); *E. coli* dTDP-glucose-4,6-dehydratase (dTDP-Glc dehydratase); *E. coli* ADP-glycero-mannoheptose 6-epimerase (AGM epimerase); *S. thyphi* CDP-tyvelose 2-epimerase (CDP-tyvelose epimerase); *A. thaliana* UDP-glucose sulfotransferase also known as UDP-sulfoquinovose synthase (UDP-Glc sulfotransferase); *Homo sapiens* UDP-glucuronic acid decarboxylase (UDP-GlcA decarboxylase); and *E. coli* ArnA C-terminal (decarboxylase) domain (ArnA C terminus). The catalytic residues S/T, Y, and K, and the NAD-binding glycine-rich motif GXXGXXG are shaded in red. Other strictly conserved residues are shaded in dark orange, while less conserved residues are shaded in light orange and yellow. The serine and arginine residues that we propose to be involved in decarboxylation are shaded in green. The corresponding residues in other proteins are shaded in blue.

active site highlights many similarities but also reveals some striking differences. Residues 178−200 in ecGALE define a long loop that lines the NAD^+-binding site but makes no contacts with the ligand. The same region in ArnA (residues 491−510) is in a completely different conformation with the loop occupying the space where NAD^+ would bind (high-

lighted in magenta in parts A and B of Figure 5). Thus, the NAD^+-binding site appears closed in ArnA, while the UDP-GlcA-binding site appears open. In contrast to ecGALE, where the NAD^+ is tightly bound to the enzyme at all times (*36*), the structure of ArnA decarboxylase suggests a model in which UDP-GlcA binds first and induces a conformational change in the enzyme that opens the binding site for NAD^+. Further experimentation is needed to test this hypothesis.

The loop defined by amino acids 31−38 in ecGALE makes close contacts with the adenine base, the ribose, and the α phosphate of NAD^+ with residues D_{31}, N_{32}, N_{35}, and S_{36}, contributing several hydrogen bonds for its binding (Figure 6) (*36*−*38*). In the corresponding region of ArnA, however, there is a four amino acid deletion in the loop (residues 348−350) that would prevent contact with the NAD^+ (colored in gold in Figures 5 and 6). This would result in lower affinity binding of NAD^+ to ArnA, which is in agreement with the different use of NAD^+ by the two enzymes. In ecGALE, the NAD^+ is used as a cofactor that is regenerated during the reaction cycle (Figure 2) and remains tightly bound to the enzyme [there are 35 protein/dinucleotide contacts in ecGALE (*38*)]. In contrast, ArnA uses NAD^+ as a substrate for the oxidation of UDP-GlcA and releases NADH as a product that would require weaker binding of NADH relative to NAD^+.

Other conformational differences between ecGALE and ArnA decarboxylase, which include amino acid insertions and deletions, occur in areas distant from the active site and do not have any obvious functional significance at this time.

Putative Catalytic Residues in ArnA Decarboxylase. The current model for the catalytic mechanism of UDP-sugar 4-epimerases, such as ecGALE, requires ring flipping of the 4-keto-sugar intermediate, which is accomplished by rotation about the bond linking the sugar α anomeric oxygen and the β phosphorus of UDP (Figure 2B). The active site of these enzymes is large enough to accommodate the reorientation of the sugar. The decarboxylation reaction catalyzed by ArnA does not require ring flipping (Figure 2A). Only one orientation of the sugar ring is likely to place the C6″ carboxylate in the active site of the enzyme. In our model of UDP-GlcA bound to ArnA, the side chain of residue E_{434} is positioned such that it would prevent flipping of the glucuronic acid ring. This glutamate is strictly conserved in all UDP-GlcA decarboxylases (see the Supporting Information). The smaller residues (serine, threonine, or alanine) found at this position in UDP-sugar 4-epimerases provide additional space in the active site, which would allow ring flipping.

When the structures of the GALE enzymes from various sources were compared with the structure of WbpP (a UDP-GlcNAc 4-epimerase), Berghuis and co-workers identified residues that determine UDP-sugar specificity in these SDR enzymes (*43*). They found that the relatively large side chains of residues K_{84}, N_{199}, and Y_{299} in ecGALE form a binding pocket, which accommodates UDP-Glc/Gal but not the larger substrates UDP-GlcNAc/GalNAc. The corresponding positions in WbpP are occupied by the smaller residues G_{102}, A_{209}, and S_{306}, making for a larger binding site, which can accommodate both UDP-GlcNAc/GalNAc and UDP-Glc/Gal. In fact, WbpP is much more efficient at catalyzing the epimerization of the *N*-acetylated sugars than the smaller, non-*N*-acetylated ones, suggesting that the binding site in WbpP is too big to constrain the conformation of UDP-Glc/Gal to a catalytically favorable orientation (*43*). In ArnA decarboxylase, the three positions discussed above are occupied by A_{393}, R_{510}, and R_{619}. Our modeling of UDP-GlcA binding to ArnA suggest that the large side chains of the arginines would not permit the binding of 2-*N*-acetylated substrates and are likely to constrain the conformation of the UDP-GlcA substrate.

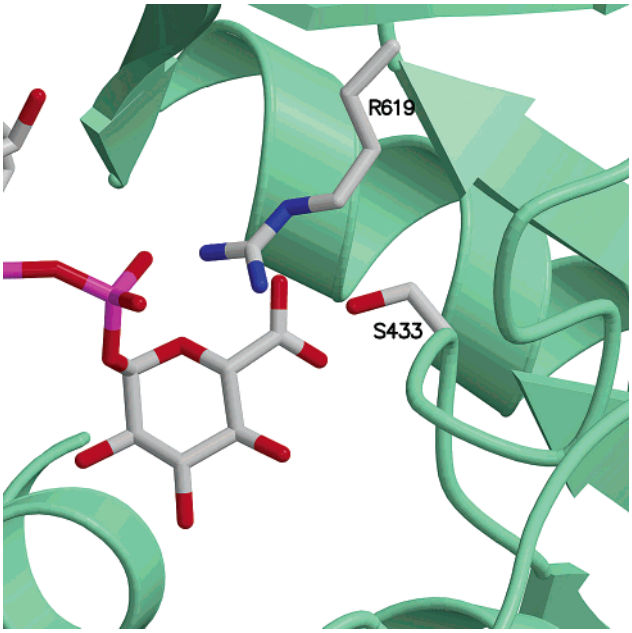

FIGURE 8: Arrangement of R_{619} and S_{433} in the vicinity of the UDP-GlcA carboxylate. The strict conservation of these residues in decarboxylases reveals their potential importance for the decarboxylation reaction.

The residue Y_{299} in ecGALE interacts with the C6″ position of UDP-Glc and, as discussed above, is important to define the sugar-nucleotide specificity of the enzyme. Mutational studies revealed that a Y299C substitution (Cys is the residue at that position in human GALE) decreased the activity with regard to UDP-galactose about 5-fold and increased the activity toward UDP-GalNAc about 230-fold (*40*). The human GALE naturally has a cysteine at that position and can also catalyze the epimerization of UDP-GalNAc (the human epimerase substrate) (*44*). A multiple sequence alignment of various SDR family members with known structures shows that the position occupied by Y_{299} in ecGALE is typically a noncharged residue. However, that position is an arginine in ArnA decarboxylase (R_{619}) and in UDP-GlcA decarboxylases (highlighted in blue and green in Figure 7). These UDP-GlcA decarboxylases (also known as UDP-xylose synthases) catalyze a reaction slightly different from ArnA in that they use NAD^+ for a complete reaction cycle (*45*−*48*). After the 4″-OH of the sugar is oxidized and the resulting 4-keto acid is decarboxylated (as in ArnA), the eukaryotic UDP-GlcA decarboxylases use NADH to re-reduce the 4-keto back to an alcohol producing UDP-xylose (Figure 2C).

In our model of ArnA decarboxylase with UDP-GlcA bound, R_{619} is well-positioned to interact with the C6″-carboxylate of UDP-glucuronic acid (Figure 8). According to our model, the side chain of S_{433} would also be poised to interact with the carboxylate of UDP-GlcA. The S_{433} position in ArnA is also a serine in UDP-GlcA decarboxylases

(highlighted in blue and green in Figure 7). That position is occupied by an aspartate in dTDP-Glc-4,6-dehydratases and has been shown to play an important role in the reaction mechanism of these enzymes (*49*−*51*).

A multiple sequence alignment of ArnA decarboxylase with every enzyme in the GeneBank annotated as UDP-GlcA decarboxylase shows that only 13.6% of the residues are conserved across all proteins (see the Supporting Information). In this context, it is striking that R_{619} and S_{433} in ArnA are among the strictly conserved residues. We therefore propose that residues R_{619} and S_{433} are important for the decarboxylase activity of ArnA. This hypothesis is supported by (i) the strict conservation of these residues in all enzymes catalyzing UDP-GlcA decarboxylation, (ii) the correct positioning of the side chains for interaction with the carboxylate of UDP-GlcA in our model of ArnA with substrates bound, and (iii) the important roles in substrate binding and catalysis played by residues in the same positions in other SDR enzymes.

Given the requirement of ArnA in the biosynthesis of Ara4N-lipid A and bacterial resistance to CAMP antimicrobials, a detailed understanding of the enzyme structure and mechanism is important. The structure of ArnA decarboxylase presented here and the accompanying hypothesis provide an excellent platform for detailed structure−function studies that may help in the design of selective inhibitors.

ACKNOWLEDGMENT

We thank Sandra Metzner for excellent technical assistance. We thank Dr. C. R. Raetz for generously providing the expression plasmid for full-length ArnA. This work is supported in part by a grant from the William M. Keck Foundation to the University of Colorado.

SUPPORTING INFORMATION AVAILABLE

Supporting Figure 1: Sequence alignment of ArnA decarboxylase with every enzyme in the GeneBank annotated as UDP-GlcA decarboxylase. Supporting Movie. Superposition of ArnA decarboxylase with UDP-galactose 4-epimerase (PDB ID: 1A9Y) showing structurally conserved regions in the two enzymes. The α carbons used for calculating rms deviation between the two proteins are colored in magenta. Additional ArnA decarboxylase residues are colored in cyan and UDP-galactose 4-epimerase residues, in gold. The UDP-Glc is shown in dark blue, and NAD^+ is colored in dark gray. This material is available free of charge via the Internet at http://pubs.acs.org.

REFERENCES

1. Hoffmann, J. A., Kafatos, F. C., Janeway, C. A., and Ezekowitz, R. A. (1999) Phylogenetic perspectives in innate immunity, *Science 284*, 1313−1318.
2. Scott, M. G., and Hancock, R. E. (2000) Cationic antimicrobial peptides and their multifunctional role in the immune system, *Crit. Rev. Immunol. 20*, 407−431.
3. Zasloff, M. (2002) Antimicrobial peptides of multicellular organisms, *Nature 415*, 389−395.
4. Zasloff, M. (1992) Antibiotic peptides as mediators of innate immunity, *Curr. Opin. Immunol. 4*, 3−7.
5. Gunn, J. S., Ryan, S. S., Van Velkinburgh, J. C., Ernst, R. K., and Miller, S. I. (2000) Genetic and functional analysis of a PmrA-PmrB-regulated locus necessary for lipopolysaccharide modification, antimicrobial peptide resistance, and oral virulence of *Salmonella enterica* serovar typhimurium, *Infect Immun. 68*, 6139−6146.
6. Gunn, J. S. (2001) Bacterial modification of LPS and resistance to antimicrobial peptides, *J. Endotoxin Res. 7*, 57−62.
7. Matsuzaki, K. (1999) Why and how are peptide−lipid interactions utilized for self-defense? Magainins and tachyplesins as archetypes, *Biochim. Biophys. Acta 1462*, 1−10.
8. Yang, L., Weiss, T. M., Lehrer, R. I., and Huang, H. W. (2000) Crystallization of antimicrobial pores in membranes: Magainin and protegrin, *Biophys. J. 79*, 2002−2009.
9. Shai, Y. (1999) Mechanism of the binding, insertion, and destabilization of phospholipid bilayer membranes by α-helical antimicrobial and cell non-selective membrane-lytic peptides, *Biochim. Biophys. Acta 1462*, 55−70.
10. Giacometti, A., Cirioni, O., Barchiesi, F., and Scalise, G. (2000) In-vitro activity and killing effect of polycationic peptides on methicillin-resistant *Staphylococcus aureus* and interactions with clinically used antibiotics, *Diagn. Microbiol. Infect. Dis. 38*, 115−118.
11. Darveau, R. P., Cunningham, M. D., Seachord, C. L., Cassiano-Clough, L., Cosand, W. L., Blake, J., and Watkins, C. S. (1991) *β*-lactam antibiotics potentiate magainin 2 antimicrobial activity in vitro and in vivo, *Antimicrob. Agents Chemother. 35*, 1153−1159.
12. Guo, L., Lim, K. B., Gunn, J. S., Bainbridge, B., Darveau, R. P., Hackett, M., and Miller, S. I. (1997) Regulation of lipid A modifications by *Salmonella typhimurium* virulence genes *phoP-phoQ*, *Science 276*, 250−253.
13. Roland, K. L., Martin, L. E., Esther, C. R., and Spitznagel, J. K. (1993) Spontaneous pmrA mutants of *Salmonella typhimurium* LT2 define a new two-component regulatory system with a possible role in virulence, *J. Bacteriol. 175*, 4154−4164.
14. Roland, K. L., and Spitznagel, J. K. (1995) Molecular genetics of polymyxin resistance in *Salmonella typhimurium*, *Prog. Clin. Biol. Res. 392*, 3−14.
15. Shafer, W. M., Casey, S. G., and Spitznagel, J. K. (1984) Lipid A and resistance of *Salmonella typhimurium* to antimicrobial granule proteins of human neutrophil granulocytes, *Infect. Immun. 43*, 834−838.
16. Ernst, R. K., Yi, E. C., Guo, L., Lim, K. B., Burns, J. L., Hackett, M., and Miller, S. I. (1999) Specific lipopolysaccharide found in cystic fibrosis airway *Pseudomonas aeruginosa*, *Science 286*, 1561−1565.
17. Peschel, A. (2002) How do bacteria resist human antimicrobial peptides? *Trends Microbiol. 10*, 179−186.
18. Gunn, J. S., Ernst, R. K., McCoy, A. J., and Miller, S. I. (2000) Constitutive mutations of the *Salmonella enterica* serovar Typhimurium transcriptional virulence regulator phoP, *Infect. Immun. 68*, 3758−3762.
19. Zhou, Z., Lin, S., Cotter, R. J., and Raetz, C. R. (1999) Lipid A modifications characteristic of *Salmonella typhimurium* are induced by NH4VO3 in *Escherichia coli* K12. Detection of 4-amino-4-deoxy-L-arabinose, phosphoethanolamine, and palmitate, *J. Biol. Chem. 274*, 18503−18514.
20. Breazeale, S. D., Ribeiro, A. A., and Raetz, C. R. (2002) Oxidative decarboxylation of UDP-glucuronic acid in extracts of polymyxin-resistant *Escherichia coli*. Origin of lipid a species modified with 4-amino-4-deoxy-L-arabinose, *J. Biol. Chem. 277*, 2886−2896.
21. Breazeale, S. D., Ribeiro, A. A., and Raetz, C. R. (2003) Origin of lipid A species modified with 4-amino-4-deoxy-L-arabinose in polymyxin-resistant mutants of *Escherichia coli*. An aminotransferase (ArnB) that generates UDP-4-deoxyl-L-arabinose, *J. Biol. Chem. 278*, 24731−24739.
22. Trent, M. S., Ribeiro, A. A., Doerrler, W. T., Lin, S., Cotter, R. J., and Raetz, C. R. (2001) Accumulation of a polyisoprene-linked amino sugar in polymyxin-resistant *Salmonella typhimurium* and *Escherichia coli*: Structural characterization and transfer to lipid A in the periplasm, *J. Biol. Chem. 276*, 43132−43144.
23. Trent, M. S., Ribeiro, A. A., Lin, S., Cotter, R. J., and Raetz, C. R. (2001) An inner membrane enzyme in *Salmonella* and *Escherichia coli* that transfers 4-amino-4-deoxy-L-arabinose to lipid A: Induction on polymyxin-resistant mutants and role of a novel lipid-linked donor, *J. Biol. Chem. 276*, 43122−43131.
24. Baker, S. J., Gunn, J. S., and Morona, R. (1999) The *Salmonella typhi* melittin resistance gene *pqaB* affects intracellular growth in PMA-differentiated U937 cells, polymyxin B resistance, and lipopolysaccharide, *Microbiology 145* (Part 2), 367−378.

25. Jornvall, H. (1999) Multiplicity and complexity of SDR and MDR enzymes, *Adv. Exp. Med. Biol. 463*, 359−364.
26. Jornvall, H., Persson, B., Krook, M., Atrian, S., Gonzalez-Duarte, R., Jeffery, J., and Ghosh, D. (1995) Short-chain dehydrogenases/reductases (SDR), *Biochemistry 34*, 6003−6013.
27. Otwinowski, Z., and Minor, W. (1997) Processing of X-ray diffraction data collected in oscillation mode, *Methods Enzymol. 276*, 307−326.
28. Thoden, J. B., Gulick, A. M., and Holden, H. M. (1997) Molecular structures of the S124A, S124T, and S124V site-directed mutants of UDP-galactose 4-epimerase from *Escherichia coli*, *Biochemistry 36*, 10685−10695.
29. Navaza, J. (2001) Implementation of molecular replacement in AMoRe, *Acta Crystallogr., Sect. D 57*, 1367−1372.
30. Brunger, A. T., Adams, P. D., Clore, G. M., DeLano, W. L., Gros, P., Grosse-Kunstleve, R. W., Jiang, J. S., Kuszewski, J., Nilges, M., Pannu, N. S., Read, R. J., Rice, L. M., Simonson, T., and Warren, G. L. (1998) Crystallography and NMR system: A new software suite for macromolecular structure determination, *Acta Crystallogr., Sect. D 54*, 905−921.
31. Brunger, A. T., Adams, P. D., and Rice, L. M. (1997) New applications of simulated annealing in X-ray crystallography and solution NMR, *Structure 5*, 325−336.
32. Brünger, A. T., Krukowski, A., and Erickson, J. (1990) Slow-cooling protocols for crystallographic refinement by simulated annealing, *Acta Crystallogr., Sect. A 46*, 585−593.
33. Jones, A. (1978) A graphics model building and refinement system for macromolecules, *J. Appl. Crystallogr. 11*, 268−272.
34. Laskowski, R. A., Macarthur, M. W., Moss, D. S., and Thornton, J. M. (1993) Procheck—A program to check the stereochemical quality of protein structures, *J. Appl. Crystallogr. 26*, 283−291.
35. Bottoms, C. A., Smith, P. E., and Tanner, J. J. (2002) A structurally conserved water molecule in Rossmann dinucleotide-binding domains, *Protein Sci. 11*, 2125−2137.
36. Thoden, J. B., Frey, P. A., and Holden, H. M. (1996) High-resolution X-ray structure of UDP-galactose 4-epimerase complexed with UDP-phenol, *Protein Sci. 5*, 2149−2161.
37. Thoden, J. B., Frey, P. A., and Holden, H. M. (1996) Molecular structure of the NADH/UDP-glucose abortive complex of UDP-galactose 4-epimerase from *Escherichia coli*: Implications for the catalytic mechanism, *Biochemistry 35*, 5137−5144.
38. Thoden, J. B., Frey, P. A., and Holden, H. M. (1996) Crystal structures of the oxidized and reduced forms of UDP-galactose 4-epimerase isolated from *Escherichia coli*, *Biochemistry 35*, 2557−2566.
39. Thoden, J. B., Hegeman, A. D., Wesenberg, G., Chapeau, M. C., Frey, P. A., and Holden, H. M. (1997) Structural analysis of UDP-sugar binding to UDP-galactose 4-epimerase from *Escherichia coli*, *Biochemistry 36*, 6294−6304.
40. Thoden, J. B., Henderson, J. M., Fridovich-Keil, J. L., and Holden, H. M. (2002) Structural analysis of the Y299C mutant of *Escherichia coli* UDP-galactose 4-epimerase. Teaching an old dog new tricks, *J. Biol. Chem. 277*, 27528−27534.
41. Thoden, J. B., Wohlers, T. M., Fridovich-Keil, J. L., and Holden, H. M. (2000) Crystallographic evidence for Tyr 157 functioning as the active site base in human UDP-galactose 4-epimerase, *Biochemistry 39*, 5691−5701.
42. Thoden, J. B., and Holden, H. M. (1998) Dramatic differences in the binding of UDP-galactose and UDP-glucose to UDP-galactose 4-epimerase from *Escherichia coli*, *Biochemistry 37*, 11469−11477.
43. Ishiyama, N., Creuzenet, C., Lam, J. S., and Berghuis, A. M. (2004) Crystal structure of WbpP, a genuine UDP-*N*-acetylglucosamine 4-epimerase from *Pseudomonas aeruginosa*: Substrate specificity in UDP-hexose 4-epimerases, *J. Biol. Chem. 279*, 22635−22642.
44. Thoden, J. B., Wohlers, T. M., Fridovich-Keil, J. L., and Holden, H. M. (2001) Human UDP-galactose 4-epimerase. Accommodation of UDP-*N*-acetylglucosamine within the active site, *J. Biol. Chem. 276*, 15131−15136.
45. Moriarity, J. L., Hurt, K. J., Resnick, A. C., Storm, P. B., Laroy, W., Schnaar, R. L., and Snyder, S. H. (2002) UDP-glucuronate decarboxylase, a key enzyme in proteoglycan synthesis: Cloning, characterization, and localization, *J. Biol. Chem. 277*, 16968−16975.
46. Kearns, A. E., Vertel, B. M., and Schwartz, N. B. (1993) Topography of glycosylation and UDP-xylose production, *J. Biol. Chem. 268*, 11097−11104.
47. John, K. V., Schutzbach, J. S., and Ankel, H. (1977) Separation and allosteric properties of two forms of UDP-glucuronate carboxy-lyase, *J. Biol. Chem. 252*, 8013−8017.
48. John, K. V., Schwartz, N. B., and Ankel, H. (1977) UDP-glucuronate carboxy-lyase in cultured chondrocytes, *J. Biol. Chem. 252*, 6707−6710.
49. Vogan, E. M., Bellamacina, C., He, X., Liu, H. W., Ringe, D., and Petsko, G. A. (2004) Crystal structure at 1.8 Å resolution of CDP-D-glucose 4,6-dehydratase from *Yersinia pseudotuberculosis*, *Biochemistry 43*, 3057−3067.
50. Babbitt, P. C., Mrachko, G. T., Hasson, M. S., Huisman, G. W., Kolter, R., Ringe, D., Petsko, G. A., Kenyon, G. L., and Gerlt, J. A. (1995) A functionally diverse enzyme superfamily that abstracts the α protons of carboxylic acids, *Science 267*, 1159−1161.
51. Allard, S. T., Giraud, M. F., Whitfield, C., Graninger, M., Messner, P., and Naismith, J. H. (2001) The crystal structure of dTDP-D-glucose 4,6-dehydratase (RmlB) from *Salmonella enterica* serovar Typhimurium, the second enzyme in the dTDP-L-rhamnose pathway, *J. Mol. Biol. 307*, 283−295.
52. Kraulis, P. (1991) MOLSCRIPT: A program to produce both detailed and schematic plots of protein structures, *J. Appl. Crystallogr. 24*, 946−950.
53. Merritt, E. A., and Bacon, D. J. (1997) Raster3D: Photorealistic Molecular Graphics, *Methods Enzymol. 277*, 505−524.

BI048551F